Received: 11 February 2023 | Revised: 10 October 2023 | Accepted: 5 November 2023

DOI: 10.1002/nbm.5078

RESEARCH ARTICLE

NMR IN BIOMEDICINE WILEY

Dynamic evaluation of acute lung injury using hyperpolarized ^{129}Xe magnetic resonance

Ming Zhang[1,2] | Haidong Li[1,2] | Hongchuang Li[1,2] | Xiuchao Zhao[1,2] | Xiaoling Liu[1,2] | Yeqing Han[1,2] | Xianping Sun[1,2] | Chaohui Ye[1,2] | Xin Zhou[1,2]

[1]Key Laboratory of Magnetic Resonance in Biological Systems, State Key Laboratory of Magnetic Resonance and Atomic and Molecular Physics, National Center for Magnetic Resonance in Wuhan, Wuhan Institute of Physics and Mathematics, Innovation Academy for Precision Measurement Science and Technology, Chinese Academy of Sciences-Wuhan National Laboratory for Optoelectronics, Huazhong University of Science and Technology, Wuhan, China

[2]University of Chinese Academy of Sciences, Beijing, China

Correspondence
Xin Zhou, Key Laboratory of Magnetic Resonance in Biological Systems, State Key Laboratory of Magnetic Resonance and Atomic and Molecular Physics, National Center for Magnetic Resonance in Wuhan, Wuhan Institute of Physics and Mathematics, Innovation Academy for Precision Measurement Science and Technology, Chinese Academy of Sciences-Wuhan National Laboratory for Optoelectronics, Huazhong University of Science and Technology, 30 West Xiaohongshan, Wuhan 430071, China.
Email: xinzhou@wipm.ac.cn

Funding information
Hubei Provincial Key Technology Foundation of China, Grant/Award Numbers: 2021ACA013, 2023BAA021; Key Research Program of Frontier Sciences, CAS, Grant/Award Number: ZDBS-LY-JSC004; National Key Research and Development Project of China, Grant/Award Numbers: 2018YFA0704000, 2022YFC2410000; National Natural Science Foundation of China, Grant/Award Numbers: 82127802, 21921004, 11905288, 82202119, 81930049; Scientific Instrument Developing Project of the Chinese Academy of Sciences, Grant/Award Number: YJKYYQ20200067; Youth Innovation Promotion Association, CAS, Grant/Award Numbers: 2020330, 2021330; Hubei Provincial Outstanding Youth Fund, Grant/Award Number: 2023AFA112; Strategic Priority Research Program of the Chinese Academy of Sciences, Grant/Award Number: XDB0540000

Abstract

Prognosticating acute lung injury (ALI) is challenging, in part because of a lack of sensitive biomarkers. Hyperpolarized gas magnetic resonance (MR) has unique advantages in pulmonary function measurement and can provide promising biomarkers for the assessment of lung injuries. Herein, we employ hyperpolarized ^{129}Xe MRI and generate a number of imaging biomarkers to detect the pulmonary physiological and morphological changes during the progression of ALI in an animal model. We find the measured ratio of ^{129}Xe in red blood cells to interstitial tissue/plasma (RBC/TP) is significantly lower in the ALI group on the second (0.32 ± 0.03, $p = 0.004$), seventh (0.23 ± 0.03, $p < 0.001$), and 14th (0.29 ± 0.04, $p = 0.001$) day after lipopolysaccharide treatment compared with that in the control group (0.41 ± 0.04). In addition, significant differences are also observed for RBC/TP measurements between the second and seventh day ($p = 0.001$) and between the seventh and 14th day ($p = 0.018$) in the ALI group after treatment. Besides RBC/TP, significant differences are also observed in the measured exchange time constant (T) on the second ($p = 0.038$) and seventh day ($p = 0.009$) and in the measured apparent diffusion coefficient (ADC) and alveolar surface-to-volume ratio (SVR) on the 14th day (ADC: $p = 0.009$ and SVR: $p = 0.019$) after treatment in the ALI group compared with that in the control group. These findings indicate that the parameters measured with ^{129}Xe MR can detect the dynamic changes in pulmonary structure and function in an ALI animal model.

KEYWORDS
acute lung injury, alveolar structure, gas exchange, hyperpolarized ^{129}Xe, pulmonary function

Abbreviations: ABG, arterial blood gas; ADC, apparent diffusion coefficient; ALI, acute lung injury; ARDS, acute respiratory distress syndrome; CSSR, chemical shift saturation recovery; DL_{CO}, diffusing capacity for carbon monoxide; DWI, diffusion-weighted imaging; HP ^{129}Xe, hyperpolarized ^{129}Xe; LPS, lipopolysaccharide; MR, magnetic resonance; MRS, MR spectroscopy; PEEP, positive end-expiratory pressure; PFTs, pulmonary function tests; RBC, red blood cells; SVR, alveolar surface-to-volume ratio; T, exchange time constant; TP, interstitial tissue/plasma.

Ming Zhang and Haidong Li contributed equally to this work.

1 | INTRODUCTION

Acute lung injury (ALI) is a disorder of acute inflammation that can cause the disruption of pulmonary endothelial and epithelial barriers, inducing acute hypoxic respiratory insufficiency.[1] Acute respiratory distress syndrome (ARDS) is the most severe form of ALI and it is also a major cause of morbidity and mortality among the critically ill patient population.[1,2] Almost 3 million people suffer from ARDS each year, and the mortality rate is approximately 40%.[3,4] Despite increasing efforts made in elucidating the pathophysiology of ARDS and the emergence of efficacious treatments,[3,5] prognostication remains challenging. Sensitive monitoring plays an important role in the management of patients with ARDS.[6]

ARDS is characterized by severe impairment of gas exchange. The severity of ARDS is defined by the ratio of arterial oxygen partial pressure to fractional inspired oxygen (PaO_2/FiO_2), in which the PaO_2 is usually measured using arterial blood gas (ABG) analysis.[7] But, according to multicenter data, the criteria might fail to provide a true risk assessment of patients.[8] Diffusing capacity for carbon monoxide (DL_{CO}), measured with pulmonary function tests (PFTs), has been used for the evaluation of long-term gas exchange outcomes in patients with ARDS.[9] However, both ABG and PFTs are unable to probe vasculature at the alveolar–capillary interface within the lung, although pulmonary vascular injury has long been known to be a key pathological feature of ARDS.[10] Chest computed tomography (CT) also plays an important role in the diagnosis and management of ARDS, because it can recognize ARDS by identifying pulmonary opacification.[11] However, CT can only image the pulmonary structure with high resolution and cannot quantify the gas exchange function of the lungs directly because it cannot image the gas in the lung.

Hyperpolarized (HP) ^{129}Xe MR is regarded as a powerful tool for lung disease evaluation and diagnosis.[12,13] Combined with diffusion-weighted imaging (DWI), it can quantify the lung morphology changes caused by various diseases, such as chronic obstructive pulmonary disease (COPD) and idiopathic pulmonary fibrosis (IPF). Moreover, by using the technique of chemical shift saturation recovery (CSSR) MR spectroscopy (MRS), gas exchange functional parameters at the alveolar–capillary interface can be obtained.[14–18] HP ^{129}Xe MR has been used to evaluate the impaired gas exchange function caused by ALI.[19] However, this important technique has not yet been employed for evaluating the dynamic physiological changes in the progression of ALI, especially the gas exchange function, which is critical for the treatment and management of ALI in the clinic.

Overall, sensitive dynamic assessment of gas exchange function at the alveolar–capillary interface is essential for the diagnosis and treatment of ALI. Unfortunately, current clinical techniques can hardly offer such information. Here, we utilized HP ^{129}Xe MRI to evaluate the physiological changes in the lung at different disease stages of ALI in an animal model.

2 | EXPERIMENTAL

2.1 | Ethical approval

All animal experimental protocols were approved by the Institutional Review Board and performed according to the national regulations for the Administration of Affairs Concerning Experimental Animals.

2.2 | Animal preparation

A total of 20 male Sprague Dawley rats (weight: 200 ± 20 g) were randomly divided into ALI ($n = 15$) and control groups ($n = 5$) after 7 days of acclimatization. The rats were intratracheally instilled with 0.2 mL of lipopolysaccharide (LPS) (3 mg/mL) and an equivalent amount of normal saline for the ALI and control groups,[19] respectively. The ALI group was further divided into three subgroups according to the period between the treatment and experiments, that is, subgroup ALI D2 ($n = 5$), ALI D7 ($n = 5$), and ALI D14 ($n = 5$).

PFTs, HP ^{129}Xe MR, and histological analysis were performed in sequence on the second day postnormal saline instillation for the control group, and on the second, seventh, and 14th days post-LPS instillation for the subgroups ALI D2, ALI D7, and ALI D14, respectively.

2.3 | Pulmonary function tests

PFTs were performed on each rat using a forced maneuvers system (CRFM 100, EMMS, UK). Before the experiments, the rats were tracheostomized after being anesthetized with pentobarbital sodium (35 mg/kg, intraperitoneal injection). Then a 14-G endotracheal tube was inserted into the trachea and secured with surgical thread to prevent gas leakage, and no significant leakage was observed during the experiments. Inspiratory capacity (IC), forced vital capacity (FVC), forced expiratory volume in 100 ms (FEV_{100}), and quasi-static lung compliance (C_{qs}) were obtained within 5 min.

2.4 | ^{129}Xe polarization and delivery

Isotopically enriched xenon gas (86% ^{129}Xe) was polarized via spin-exchange optical pumping using a commercial polarizer (verImagin Healthcare, Wuhan, China). HP xenon gas was cryogenically accumulated in a spiral-shaped cold trap[20,21] and then thawed into a Tedlar bag. A total of 160 mL of HP ^{129}Xe was used for each rat. During the MR experiments, 2% isoflurane was used to maintain the anesthesia, and HP xenon gas and oxygen were ventilated alternately to the rat lungs using a homebuilt MR-compatible gas delivery system via a homebuilt LabVIEW program.[21] The positive end-expiratory pressure (PEEP) was 5-cm H_2O, and the tidal volume was 2 mL.[22,23] The airway pressure was monitored in real time and was limited to less than 20-cm H_2O.

2.5 | MR experiments

All the MR experiments were performed on a 7.0-T animal MRI scanner (Bruker BioSpec 70/20 USR, Germany) equipped with a homebuilt ^{129}Xe/^{1}H dual-tuned birdcage coil. HP ^{129}Xe DWI and MRS were performed on each rat to obtain the morphological and physiological parameters, respectively.

For HP ^{129}Xe DWI, a non-slice selection diffusion-weighted gradient-echo sequence was used. The acquisition parameters were as follows: ramp-up/down time = 0.123 ms; constant time = 0.7 ms; diffusion time = 1.2 ms; matrix size = 64 × 64; field of view = 50 × 50 mm; flip angle = 10°; bandwidth = 50 kHz, and TE = 3.52 ms. Nine b values (0, 4, 8, 12, 16, 20, 24, 28, and 32 s/cm^2) were used for extracting the morphological parameters. For images with nonzero b values, three images with and without diffusion gradient (0, b, 0 s/cm^2) were acquired using an interleaved sampling strategy in a single breath-hold, as described in previous studies.[21,24]

For HP ^{129}Xe MRS, a CSSR pulse sequence was used, as previously described.[21] Briefly, two Gaussian-shaped pulses with durations of 0.5 and 0.2 ms were used to saturate and excite the dissolved ^{129}Xe signals, with off-resonance effects of 0.1° and 0.9° on gas-phase ^{129}Xe, respectively. Spectra were acquired with a bandwidth of 25 kHz and 1024 sampling points, and 24 exchange time points ranging from 2 to 400 ms were used. All spectra were repeatedly measured three times, and each measurement was performed within a single breath-hold after two xenon flushes.

2.6 | Data processing

All the data were processed in Matlab software (MathWorks, Natick, MA, USA). The raw data of HP ^{129}Xe DWI were reconstructed into images by two-dimensional Fourier transform. For the three images acquired within the same breath-hold, two images without diffusion weight were averaged and then were used to generate the binary mask to segment the image with diffusion weight. After that, pixels with a signal-to-noise ratio of less than 3 were excluded, and the main tracheal was removed by the seed-growing algorithm.[24] Next, images with b = 0 and 12 s/cm^2 were used to calculate the apparent diffusion coefficient (ADC) map using the monoexponential model, and images with b = 0–32 s/cm^2 were used to fit with a diffusion model to extract the morphological parameters,[25] including the alveolar surface-to-volume ratio (SVR) and alveolar mean chord length (Lm).

For HP ^{129}Xe MRS, spectra were fitted to the Lorentzian shape to extract the signal amplitudes of ^{129}Xe in interstitial tissue/plasma (TP), red blood cells (RBC), and the gas phase, respectively. Signal amplitudes of TP and RBC were first normalized by the gas phase signal then fitted to the model of xenon exchange (MOXE) to extract the physiological parameters,[20,21] including the exchange time constant (T), septal wall thickness (d), and blood hematocrit (Hct).[26] In addition, signal amplitudes of RBC, TP, and gas phase in spectra with an exchange time of 100 ms were used to obtain the ratios of RBC/Gas, TP/Gas, and RBC/TP.[20,21]

2.7 | Quantitative histology

After the experiments, the lung was extracted immediately after the rats were euthanized. The extracted lungs were instilled with 4% paraformaldehyde with a pressure of 25-cm H_2O for more than 2 h then kept in the same solution for 48 h. Paraffin-embedded lung was cut into 5-μm-thick tissue sections then stained with hematoxylin and eosin (H&E) and Masson's trichrome (for assessing the fibrosis). Images that did not contain the large airway were acquired with a microscope (Nikon Eclipse TS100, Japan) for each section.[24] The alveolar septal thickness was calculated automatically using a homebuilt Matlab program. A standard test grid was then overlaid on the images, and the septal thickness was determined as the average of the total truncated length.[27,28]

2.8 | Statistical analysis

Unpaired *t*-tests were used to compare the parameters measured with PFTs, ^{129}Xe MR, and quantitative histology for the control and ALI groups and for ALI subgroups. Moreover, the Pearson correlation coefficient (*r*) was used to determine the relationship between septal wall thickness measured with HP ^{129}Xe MRS and quantitative histology. All the statistical analyses were performed using PASW Statistics 18 (SPSS, Chicago, IL, USA). *p* values less than 0.05 were considered statistically significant.

3 | RESULTS

3.1 | Pulmonary function tests

Significant differences were found in measured IC, FVC, and C_{qs} between subgroup ALI D14 and the control group (IC: $p = 0.044$; FVC: $p = 0.022$; C_{qs}: $p = 0.029$). IC and FVC also showed significances between subgroups ALI D14 and ALI D7 (IC: $p = 0.009$; FVC: $p = 0.022$). Moreover, FEV_{100} was higher in subgroup ALI D14 than in subgroup ALI D7 with significance ($p = 0.008$). However, no significant differences were observed in the measured PFT parameters between the control group and subgroup ALI D2, the control group and subgroup ALI D7, and subgroups ALI D2 and ALI D7, as shown in Table 1.

3.2 | Hyperpolarized ^{129}Xe DWI

Figure 1 shows representative ADC and morphological maps from the control and ALI groups. Substantially higher ADC, Lm, and lower SVR can be observed in subgroup ALI D14 versus the control group; quantitative results of the measured morphological parameters from all groups are

TABLE 1 Summary of the physiological and morphological parameters measured with PFTs, hyperpolarized ^{129}Xe DWI, and MRS.

		ALI			Statistics				
Parameters	Ctrl.	D2	D7	D14	Ctrl. vs. D2	Ctrl. vs. D7	Ctrl. vs. D14	D2 vs. D7	D7 vs. D14
PFTs									
IC (mL)	8.52 (1.36)	6.53 (2.53)	6.72 (2.15)	10.52 (1.30)	0.160	0.151	**0.044***	0.905	**0.009***
FVC (mL)	10.40 (1.28)	8.36 (2.61)	8.74 (2.89)	12.84 (1.43)	0.155	0.273	**0.022***	0.835	**0.022***
FEV_{100} (mL)	4.03 (0.99)	3.44 (0.62)	2.95 (0.77)	4.23 (0.28)	0.297	0.090	0.669	0.291	**0.008***
C_{qs} (mL/cm H_2O)	0.90 (0.19)	0.79 (0.31)	0.85 (0.28)	1.14 (0.08)	0.512	0.776	**0.029***	0.725	0.056
DWI									
ADC (cm^2/s)	0.0354 (0.0016)	0.0364 (0.0019)	0.0358 (0.0030)	0.0404 (0.0028)	0.422	0.821	**0.009***	0.719	**0.038***
Lm (μm)	95 (8)	99 (7)	97 (13)	108 (8)	0.444	0.797	**0.031***	0.779	0.154
SVR (cm^{-1})	441 (35)	420 (35)	434 (58)	382 (27)	0.382	0.816	**0.019***	0.679	0.126
MRS									
T (ms)	21.44 (3.35)	33.30 (10.18)	30.57 (4.35)	24.49 (5.65)	**0.038***	**0.006***	0.330	0.596	0.093
d (μm)	8.34 (0.66)	10.32 (1.54)	9.96 (0.69)	8.88 (1.02)	**0.029***	**0.005***	0.345	0.643	0.088
Hct	0.26 (0.02)	0.21 (0.01)	0.17 (0.02)	0.19 (0.02)	**0.006***	**< 0.001***	**0.002***	**0.002***	0.117
RBC/gas ($\times 10^{-2}$)	0.60 (0.05)	0.54 (0.09)	0.45 (0.13)	0.43 (0.03)	0.239	**0.041***	**< 0.001***	0.234	0.646
TP/gas ($\times 10^{-2}$)	1.49 (0.13)	1.68 (0.21)	1.98 (0.41)	1.48 (0.12)	0.131	**0.035***	0.950	0.184	**0.032***
RBC/TP	0.41 (0.04)	0.32 (0.03)	0.23 (0.03)	0.29 (0.04)	**0.004***	**< 0.001***	**0.001**	**0.001***	**0.018***

Notes: Unless otherwise indicated, data are presented as the mean (standard deviation). The *p* values were calculated between the four groups with significant differences in bold.

Abbreviations: ADC, apparent diffusion coefficient; ALI, acute lung injury; C_{qs}, quasi-static lung compliance; Ctrl., control group; d, septal wall thickness; D14, 14 days after instillation; D2, 2 days after instillation; D7, 7 days after instillation; DWI, diffusion-weighted imaging; FEV_{100}, forced expiratory volume in 100 ms; FVC, forced vital capacity; Hct, blood hematocrit; IC, inspiratory capacity; Lm, alveolar mean chord length; MRS, magnetic resonance spectroscopy; PFTs, pulmonary function tests; RBC, red blood cells; SVR, alveolar surface-to-volume ratio; T, exchange time constant; TP, interstitial tissue/plasma.

*Unpaired *t*-test, $p < 0.05$.

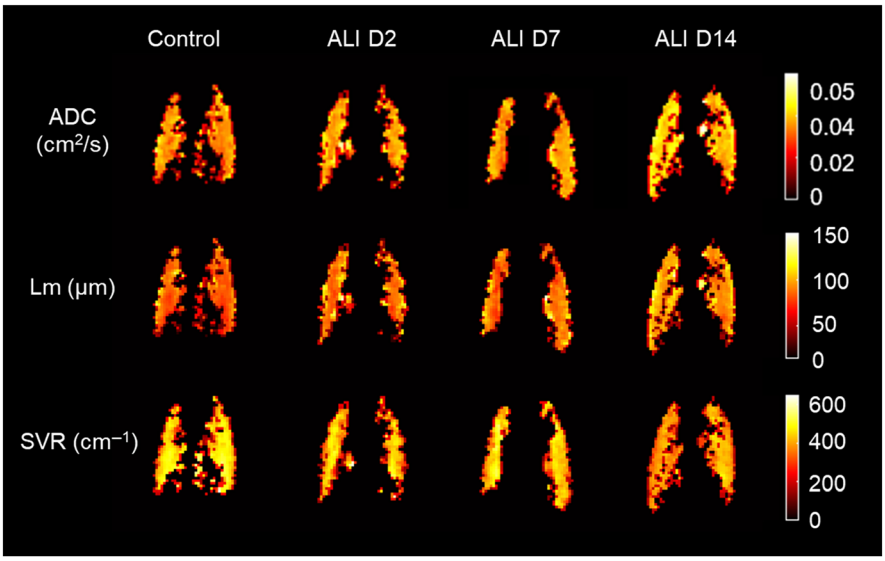

FIGURE 1 Representative ADC, Lm, and SVR maps from the control group and subgroups ALI D2, ALI D7, and ALI D14. Higher ADC, Lm, and lower SVR can be observed in subgroup ALI D14 compared with the control group. ADC, apparent diffusion coefficient; ALI, acute lung injury; D14, 14 days after instillation; D2, 2 days after instillation; D7, 7 days after instillation; Lm, alveolar mean chord length; SVR, alveolar surface-to-volume ratio.

summarized in Table 1. ADC, Lm, and SVR showed significances between the control group and subgroup ALI D14 (ADC: $p = 0.009$, Lm: $p = 0.031$ and SVR: $p = 0.019$).

3.3 | Hyperpolarized ^{129}Xe MRS

Figure 2 shows the representative dissolved xenon recovery curves measured from each group. Dissolved xenon signals obviously recovered more slowly in subgroup ALI D7, wherein the normalized TP signal was significantly higher compared with that in the control group. Moreover, xenon signal recovery curves in subgroup ALI D14 were similar to those in the control group.

Figure 3 shows the comparisons of the physiological parameters derived with HP ^{129}Xe MRS among the groups. Significant differences were observed in the measured T, d, and Hct between subgroup ALI D2 and the control group (T: $p = 0.038$; d: $p = 0.029$; Hct: $p = 0.006$), and subgroup ALI D7 and the control group (T: $p = 0.006$; d: $p = 0.005$; Hct: $p < 0.001$). Moreover, significant differences were also observed in Hct between the control group and subgroup ALI D14 ($p = 0.002$) and between the subgroups ALI D2 and ALI D7 ($p = 0.002$). In addition, the highest T and d measurements were found in subgroup ALI D2, and the lowest Hct was observed in subgroup ALI D7.

Figure 4 shows the comparisons of the dissolved signals at the exchange time of 100 ms among the groups. RBC/TP showed significant differences between the control group and subgroup ALI D2 ($p = 0.004$), the control group and subgroup ALI D7 ($p < 0.001$), the control group and subgroup ALI D14 ($p = 0.001$), subgroups ALI D2 and ALI D7 ($p = 0.001$), and subgroups ALI D7 and ALI D14 ($p = 0.018$). Moreover, significant differences were observed in RBC/gas between the control group and subgroup ALI D7 ($p = 0.041$) and the control group and subgroup ALI D14 ($p < 0.001$). Significant differences were also observed in TP/gas between the control group and subgroup ALI D7 ($p = 0.035$) and subgroups ALI D7 and ALI D14 ($p = 0.032$). After being treated with LPS, RBC/gas decreased with time, TP/gas increased first and then decreased, and RBC/TP decreased first and then increased. In addition, the highest TP/gas and lowest RBC/TP were observed in subgroup ALI D7. The results are also summarized in Table 1.

3.4 | Histological observations

Figure 5 shows the representative histological sections from all groups, and the collagen deposition was stained in blue in Masson's trichrome stained images. Severe neutrophil infiltration can be observed in subgroup ALI D2, and thickened septal wall thickness and collagen deposition that spreads throughout the lung can be observed in subgroup ALI D7, indicating pulmonary fibrosis. Moreover, collagen deposition and enlarged alveolar sizes were observed in subgroup ALI D14, although neutrophil infiltration and thickened septal wall were not observed. The septal wall thickness measured with histology was 5.91 ± 0.38, 8.26 ± 1.13, 8.12 ± 0.43, and 6.76 ± 0.74 μm for the control group and subgroups ALI D2, ALI D7,

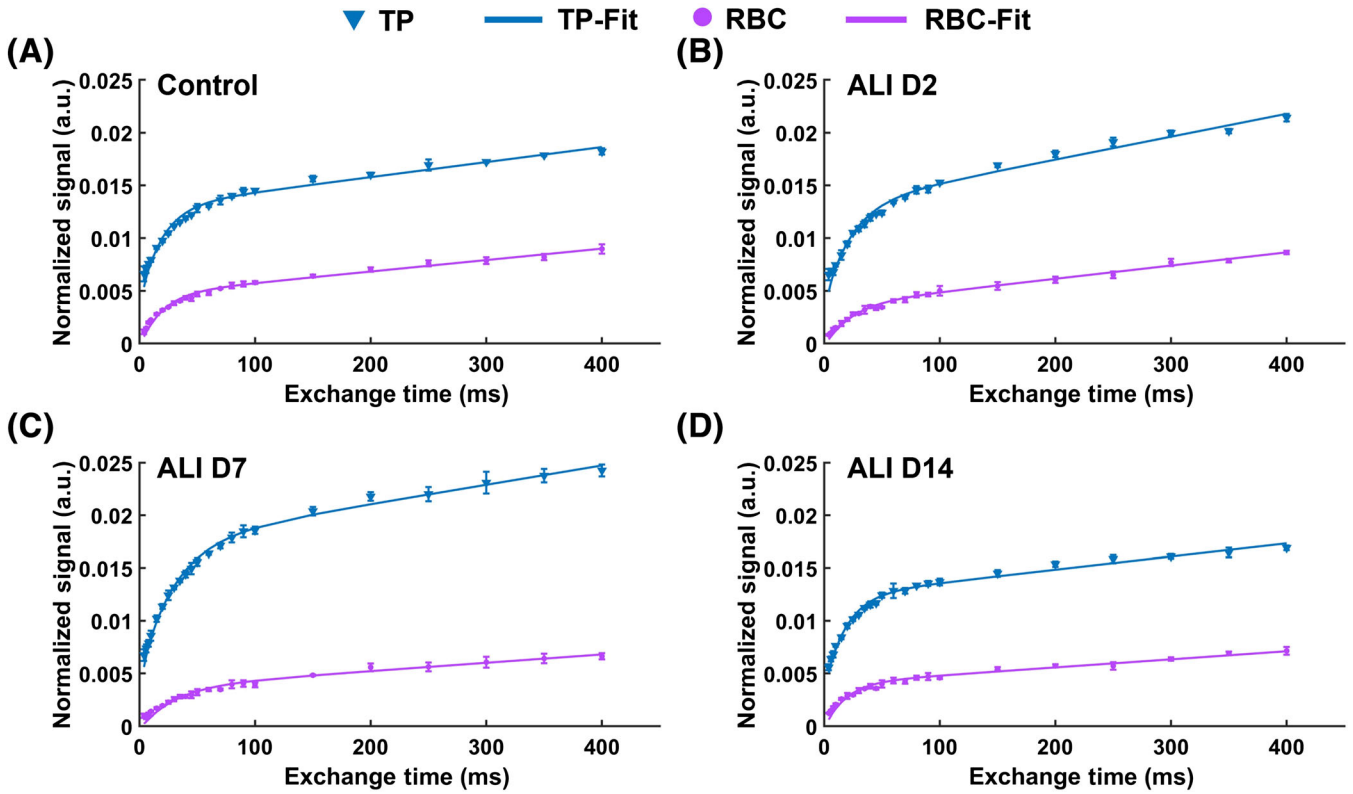

FIGURE 2 Typical dissolved xenon signal recovery curves for each group. Compared with the control group (A), the recovery of RBC and TP ^{129}Xe signal was slower in subgroup ALI D2 (B). Of all the groups, the recovery of dissolved xenon signal was slowest in subgroup ALI D7 (C), and the TP signal was obviously higher than that in the other groups. Subgroup ALI D14 (D) has similar dissolved xenon signal recovery curves as those in the control group. Each point on the curves is an average of three separate experiments. ALI, acute lung injury; D14, 14 days after instillation; D2, 2 days after instillation; D7, 7 days after instillation; RBC, red blood cells; TP, interstitial tissue/plasma.

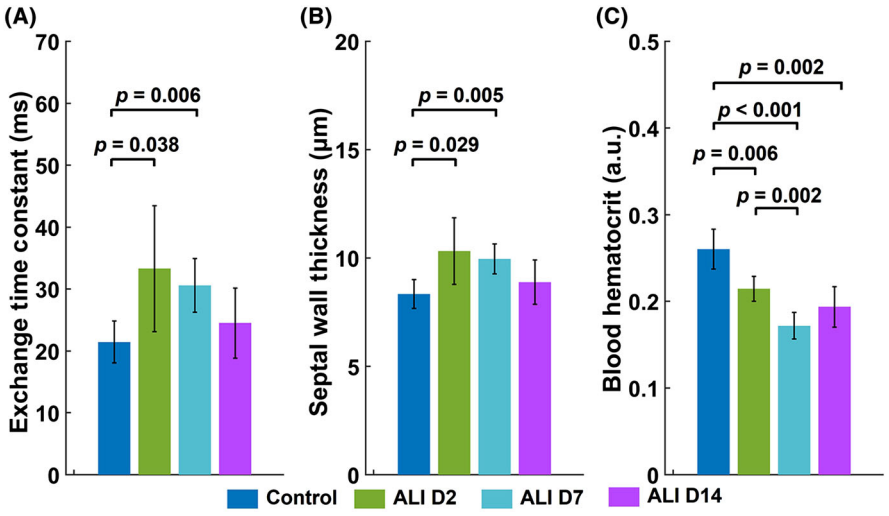

FIGURE 3 Comparisons of the physiological parameters derived with ^{129}Xe MRS among the groups. Compared with the control group, both the exchange time constant (A) and septal wall thickness (B) increased first and then decreased after the rats were treated with LPS. On the contrary, blood hematocrit (C) decreased first and then increased. ALI, acute lung injury; D14, 14 days after instillation; D2, 2 days after instillation; D7, 7 days after instillation; LPS, lipopolysaccharide.

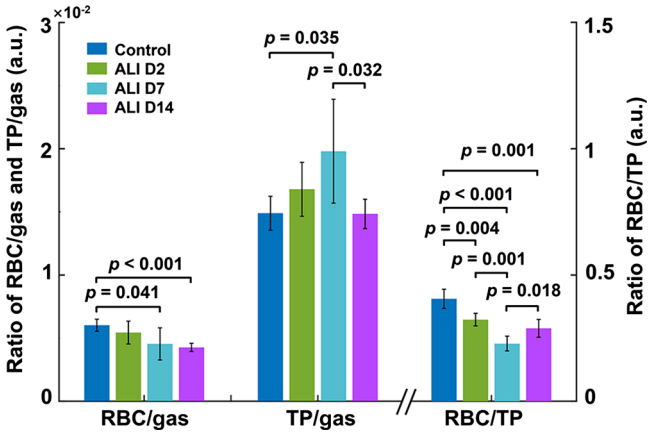

FIGURE 4 Comparisons of RBC/gas, TP/gas, and RBC/TP among the groups. Compared with the control group, RBC/gas decreased with the progression of ALI, and TP/gas increased first and then decreased. Moreover, RBC/TP decreased first and then increased after the rats were treated with LPS. RBC/TP showed significant differences between the groups. ALI, acute lung injury; D14, 14 days after instillation; D2, 2 days after instillation; D7, 7 days after instillation; LPS, lipopolysaccharide; RBC, red blood cells; TP, interstitial tissue/plasma.

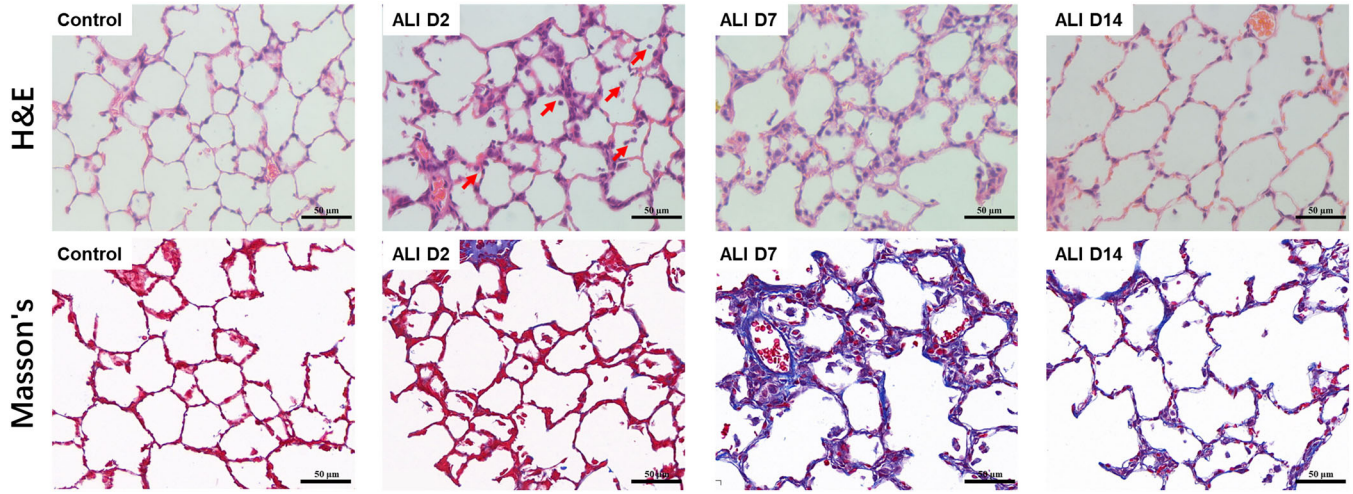

FIGURE 5 H&E and Masson's trichrome stained histological images of the representative rats from the control and ALI groups (scale bar = 50 μm). Compared with the control group, the inflammation (red arrows in the H&E-stained image) and alveolar disruption can be observed in subgroup ALI D2, and obvious thickening of the septal wall and obvious collagen deposition can be observed in subgroup ALI D7. In subgroup ALI D14, the enlarged alveolar and collagen deposition can be observed, although the inflammation and thickened septal wall were resolved. ALI, acute lung injury; D14, 14 days after instillation; D2, 2 days after instillation; D7, 7 days after instillation; H&E, hematoxylin and eosin.

and ALI D14, respectively. Significant differences were observed between the control group and subgroup ALI D2 ($p = 0.007$) and the control group and subgroup ALI D7 ($p < 0.001$). Moreover, the measured septal wall thickness showed a good correlation with that using quantitative histology, as shown in Figure 6.

4 | DISCUSSION

In this study, the physiological changes in an animal model of ALI were dynamically assessed using HP ^{129}Xe MR, and promising biomarkers were proposed. Our preliminary results showed that pulmonary function deteriorated first and then recovered in the ALI group after LPS treatment, and that the ratio of ^{129}Xe in red blood cells to interstitial tissue/plasma (i.e., RBC/TP) may serve as a promising biomarker for quantifying the physiological changes during the progression of ALI in the animal model. Moreover, the measurements of the gas exchange time constant (T) and ADC were sensitive to the short- and long-term outcomes of ALI, respectively. These findings showed that, using an animal model of ALI,

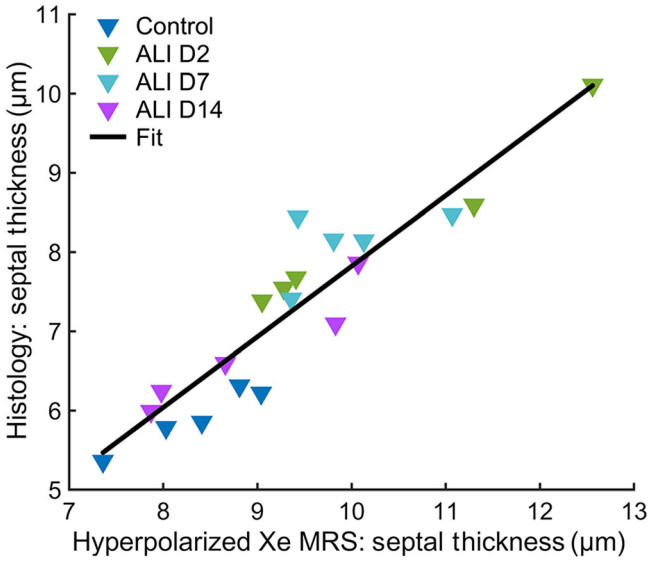

FIGURE 6 Correlation of the septal thickness derived by ^{129}Xe MRS and quantitative histology ($p < 0.001$, $r = 0.928$). The solid line is the linear fit of the two methods. ALI, acute lung injury; D14, 14 days after instillation; D2, 2 days after instillation; D7, 7 days after instillation; MRS, magnetic resonance spectroscopy.

functional and structural changes in the lung can be dynamically detected and quantified by HP ^{129}Xe MR with high sensitivity without ionizing radiation.

RBC/TP showed high sensitivity in the dynamic assessment of lung physiology in an ALI animal model. As a widely used ^{129}Xe MR biomarker, RBC/TP has been used for quantifying changes in gas exchange function caused by lung diseases, such as COPD, IPF, and COVID-19.[18,29,30] In this study, we found that RBC/TP decreased first and then increased in the ALI group, and the same trend was also observed in PFT measurements. However, no statistical significance was found in PFTs measurements in the short term for the ALI animal model. In addition, changes in RBC/TP were also consistent with the histological results, which indicated acute inflammation on the second day and fibrosis on the seventh day after LPS treatment[21,29] and substantially resolved inflammation on the 14th day.

Exchange time constant (T) measured with ^{129}Xe MRS was a potentially sensitive biomarker for detecting the short-term abnormalities of the alveolar–capillary membrane in an ALI animal model. The measured T substantially increased in the ALI group on the second and seventh day after LPS treatment compared with the control group. These findings were similar to those reported from previous studies.[21,31,32] This may be because of the exudation and infiltration of polymorphonuclear neutrophils in lungs on the second day after LPS treatment,[33] which would make it difficult for xenon to enter into the capillary.[20,21] Then, on the seventh day, secondary fibrosis after the acute inflammation[33] would thicken the alveolar septal wall and reduce the gas exchange efficiency. On the 14th day after treatment, the measured T decreased in the ALI group, probably because the acute inflammation was resolved[31,34] and the reduced septal wall thickness made it easier for xenon to pass through.

ABG analysis and the DL_{CO} measure are widely used for assessing the lung gas exchange. ABG analysis can be used for assessing the severity of ARDS,[7] although ABG analysis is invasive, and arteries' blood is needed for obtaining the PaO_2/FiO_2 ratio. Meanwhile, it can only measure the partial pressure of oxygen and carbon dioxide and cannot measure the gas exchange in the lung directly. DL_{CO} measures the differences of carbon monoxide concentration between the gas mixture inhaled and exhaled by the patient. It can assess the ability of the lung to transfer gas from inspired air to the bloodstream, but it cannot probe the vasculature at the alveolar–capillary interface.[35] Compared with these methods, ^{129}Xe MR allows direct assessment of the lung gas exchange function by analyzing ^{129}Xe signal in alveolar, TP, and capillary RBC. The derived parameters from CSSR, such as hematocrit and RBC/gas ratio, can be used for evaluating the gas exchange function at the alveolar–capillary interface, which can hardly be obtained using clinical methods without invasion.[35,36]

ADC and morphological parameters measured with ^{129}Xe DWI suggest the potential of HP ^{129}Xe MRI for assessing the long-term alveolar structural changes in ALI. The increased ADC and Lm and decreased SVR on the 14th day after LPS treatment suggested the increase of the alveolar sizes and agreed with the results of PFTs and histological analysis. These emphysema-like injuries were similar to those reported in previous studies.[31,37,38] No significant differences were observed in the measured ADC and morphological parameters on the second and seventh day after LPS treatment compared with the control group. This was probably because of the simultaneous existence of acute inflammation and emphysema-like changes. The inflammation would lead to a decrease in the alveolar size,[39] but emphysema-like changes would cause an increase in the alveolar size.[38]

To investigate the progression of ALI, the lung injury model was induced by intratracheal instillation of LPS in our study. As one of the most widely used rodent models of acute lung inflammation, the responses of the lungs to injury would change with time in the short-term effect of LPS,[40] while for the long-term effect of LPS, some studies have shown that the inflammation would be resolved and the lung could recover from injury.[31,41] Such characteristics are similar to the reparative processes of ALI in humans.[34] To depict the dynamic development of ALI, different rats were used for each time point. A similar design has also been commonly used in animal experiments for studying the disease process.[31,41]

Our research can be extended in several ways. Endotracheal intubation with tracheostomy was used in this study, and rats would be euthanized after examinations, which hinders the longitudinal study on the same rats. Instead, we used five different rats from the ALI group at different times post-LPS instillation, a strategy widely used in animal studies for assessing progression.[34,42] Next, three time points were chosen after the rats were treated with LPS according to the previous study[31]; however, these time points may not fully depict the development of ALI, and more time points are needed for a comprehensive understanding of LPS-induced ALI. Furthermore, the gas exchange function was measured globally with MRS in this study, and local assessment of the gas exchange function should also be included in future studies. Given the potential alveolar collapse in the ALI model, a meticulous ADC protocol that incorporates PEEP and recruitment maneuver may be employed in future studies to minimize the biases in ADC measurements. Lastly, although dynamic changes in lung physiological function were observed through ^{129}Xe MR in the ALI animal model, further studies are needed to determine the applicability of this technique for evaluating ALI in the clinic. On the one hand, whether the observed lung physiological changes are unique to ALI warrants further investigation. On the other hand, the applications of ^{129}Xe MRI for the assessment of critically ill patients in the clinic remains a challenge, particularly for those patients requiring mechanical ventilation who cannot leave the intensive care unit, and customized hardware and pulse sequences tailored to these patients are needed.

5 | CONCLUSIONS

In summary, we employed HP ^{129}Xe MR to evaluate the progression of lung structural and functional changes in vivo in an animal model of ALI induced by LPS. Our results showed that RBC/TP can sensitively and dynamically assess the gas exchange function changes, T can assess the short-term functional changes, and ADC can assess the long-term alveolar structural changes. These findings may support the use of HP ^{129}Xe MR in future clinical studies of ALI.

ACKNOWLEDGMENTS

This work is supported by the National Key Research and Development Project of China (2018YFA0704000, 2022YFC2410000), National Natural Science Foundation of China (82127802, 21921004, 11905288, 82202119, 81930049), Scientific Instrument Developing Project of the Chinese Academy of Sciences (YJKYYQ20200067), Key Research Program of Frontier Sciences, CAS (ZDBS-LY-JSC004), Hubei Provincial Key Technology Foundation of China (2021ACA013, 2023BAA021), Hubei Provincial Outstanding Youth Fund (2023AFA112), and Strategic Priority Research Program of the Chinese Academy of Sciences (XDB0540000). Haidong Li and Xiuchao Zhao acknowledge the support from the Youth Innovation Promotion Association, CAS (2020330, 2021330).

CONFLICT OF INTEREST STATEMENT

The authors declare that they have no conflicts of interest.

ORCID

Xin Zhou https://orcid.org/0000-0002-5580-7907

REFERENCES

1. Johnson ER, Matthay MA. Acute lung injury: epidemiology, pathogenesis, and treatment. *J Aerosol Med Pulm Drug Deliv*. 2010;23(4):243-252. doi:10.1089/jamp.2009.0775
2. Ragaller M, Richter T. Acute lung injury and acute respiratory distress syndrome. *J Emerg Trauma Shock*. 2010;3(1):43. doi:10.4103/0974-2700.58663
3. Fan E, Brodie D, Slutsky AS. Acute respiratory distress syndrome: advances in diagnosis and treatment. *JAMA*. 2018;319(7):698-710. doi:10.1001/jama.2017.21907
4. Lewis SR, Pritchard MW, Thomas CM, Smith AF. Pharmacological agents for adults with acute respiratory distress syndrome. *Cochrane Database Syst Rev*. 2019;7(7):CD004477. doi:10.1002/14651858.CD004477.pub3
5. Ware LB. Pathophysiology of acute lung injury and the acute respiratory distress syndrome. *Semin Respir Crit Care Med*. 2006;27(04):337-349. doi:10.1055/s-2006-948288
6. Brochard L, Martin GS, Blanch L, et al. Clinical review: respiratory monitoring in the ICU-a consensus of 16. *Crit Care*. 2012;16(2):1-14. doi:10.1186/cc11146
7. Force ADT, Ranieri V, Rubenfeld G, et al. Acute respiratory distress syndrome. *JAMA*. 2012;307(23):2526-2533.

8. Villar J, Pérez-Méndez L, Blanco J, et al. A universal definition of ARDS: the PaO2/FiO2 ratio under a standard ventilatory setting—a prospective, multicenter validation study. *Intensive Care Med*. 2013;39(4):583-592. doi:10.1007/s00134-012-2803-x
9. Chiumello D, Coppola S, Froio S, Gotti M. What's next after ARDS: long-term outcomes. *Respir Care*. 2016;61(5):689-699. doi:10.4187/respcare.04644
10. Blaisdell FW. Pathophysiology of the respiratory distress syndrome. *Arch Surg*. 1974;108(1):44-49. doi:10.1001/archsurg.1974.01350250036009
11. Sheard S, Rao P, Devaraj A. Imaging of acute respiratory distress syndrome. *Respir Care*. 2012;57(4):607-612. doi:10.4187/respcare.01731
12. Ruppert K, Qing K, Patrie JT, Altes TA, Mugler JP III. Using hyperpolarized xenon-129 MRI to quantify early-stage lung disease in smokers. *Acad Radiol*. 2019;26(3):355-366. doi:10.1016/j.acra.2018.11.005
13. Sharma M, Wyszkiewicz PV, Desaigoudar V, Guo F, Capaldi D, Parraga G. Quantification of pulmonary functional MRI: state-of-the-art and emerging image processing methods and measurements. *Phys Med Biol*. 2022;67(22):22TR01. doi:10.1088/1361-6560/ac9510
14. Petersson-Sjögren M, Chan H-F, Collier GJ, et al. Airspace dimension assessment (AiDA) by inhaled nanoparticles: benchmarking with hyperpolarised ^{129}Xe diffusion-weighted lung MRI. *Sci Rep*. 2021;11(1):4721. doi:10.1038/s41598-021-83975-7
15. Ouriadov AV, Fox MS, Lindenmaier AA, Stirrat E, Serrai H, Santyr G. Application of a stretched-exponential model for morphometric analysis of accelerated diffusion-weighted ^{129}Xe MRI of the rat lung. *Magn Reson Mater Phys, Biol Med*. 2021;34(1):73-84. doi:10.1007/s10334-020-00860-6
16. Wang Z, Rankine L, Bier EA, et al. Using hyperpolarized ^{129}Xe gas exchange MRI to model the regional airspace, membrane and capillary contributions to diffusing capacity. *J Appl Physiol*. 2021;130(5):1398-1409. doi:10.1152/japplphysiol.00702.2020
17. Niedbalski PJ, Cochran AS, Freeman MS, et al. Validating in vivo hyperpolarized ^{129}Xe diffusion MRI and diffusion morphometry in the mouse lung. *Magn Reson Med*. 2021;85(4):2160-2173. doi:10.1002/mrm.28539
18. Li H, Zhao X, Wang Y, et al. Damaged lung gas exchange function of discharged COVID-19 patients detected by hyperpolarized ^{129}Xe MRI. *Sci Adv*. 2021;7(1):eabc8180. doi:10.1126/sciadv.abc8180
19. Mansson S, Wolber J, Driehuys B, Wollmer P, Golman K. Characterization of diffusing capacity and perfusion of the rat lung in a lipopolysaccaride disease model using hyperpolarized ^{129}Xe. *Magn Reson Med*. 2003;50(6):1170-1179. doi:10.1002/mrm.10649
20. Li H, Zhang Z, Zhao X, Sun X, Ye C, Zhou X. Quantitative evaluation of radiation-induced lung injury with hyperpolarized xenon magnetic resonance. *Magn Reson Med*. 2016;76(2):408-416. doi:10.1002/mrm.25894
21. Zhang M, Li H, Li H, et al. Quantitative evaluation of lung injury caused by $PM_{2.5}$ using hyperpolarized gas magnetic resonance. *Magn Reson Med*. 2020;84(2):569-578. doi:10.1002/mrm.28145
22. Magalhães PA, Padilha GA, Moraes L, et al. Effects of pressure support ventilation on ventilator-induced lung injury in mild acute respiratory distress syndrome depend on level of positive end-expiratory pressure: a randomised animal study. *Eur J Anaesthesiol*. 2018;35(4):298-306. doi:10.1097/EJA.0000000000000763
23. Kollisch-Singule M, Emr B, Smith B, et al. Airway pressure release ventilation reduces conducting airway micro-strain in lung injury. *J Am Coll Surg*. 2014;219(5):968-976. doi:10.1016/j.jamcollsurg.2014.09.011
24. Ruan W, Zhong J, Wang K, et al. Detection of the mild emphysema by quantification of lung respiratory airways with hyperpolarized xenon diffusion MRI. *J Magn Reson Imaging*. 2017;45(3):879-888. doi:10.1002/jmri.25408
25. Sukstanskii AL, Yablonskiy DA. Lung morphometry with hyperpolarized ^{129}Xe: theoretical background. *Magn Reson Med*. 2012;67(3):856-866. doi:10.1002/mrm.23056
26. Chang YV. MOXE: a model of gas exchange for hyperpolarized ^{129}Xe magnetic resonance of the lung. *Magn Reson Med*. 2013;69(3):884-890. doi:10.1002/mrm.24304
27. Pua ZJ, Stonestreet BS, Cullen A, Shahsafaei A, Sadowska GB, Sunday ME. Histochemical analyses of altered fetal lung development following single vs multiple courses of antenatal steroids. *J Histochem Cytochem*. 2005;53(12):1469-1479. doi:10.1369/jhc.5A6721.2005
28. Woods JC, Choong CK, Yablonskiy DA, et al. Hyperpolarized ^{3}He diffusion MRI and histology in pulmonary emphysema. *Magn Reson Med*. 2006;56(6):1293-1300. doi:10.1002/mrm.21076
29. Eaden J, Hughes P, Collier G, et al. Longitudinal change in hyperpolarised 129-xenon MR spectroscopy in interstitial lung disease. *Eur Respir J*. 2019;54(suppl 63):PA3158. doi:10.1183/13993003.congress-2019.PA3158
30. Hahn AD, Carey KJ, Barton GP, et al. Hyperpolarized ^{129}Xe MR spectroscopy in the lung shows 1-year reduced function in idiopathic pulmonary fibrosis. *Radiology*. 2022;305(3):688-696. doi:10.1148/radiol.211433
31. Tsikis S, Fligor S, Hirsch T, et al. Lipopolysaccharide-induced murine lung injury results in long-term pulmonary changes and downregulation of angiogenic pathways. *Sci Rep*. 2022;12(1):1-12. doi:10.1038/s41598-022-14618-8
32. Wang JM, Robertson SH, Wang ZY, et al. Using hyperpolarized Xe-129 MRI to quantify regional gas transfer in idiopathic pulmonary fibrosis. *Thorax*. 2018;73(1):21-28. doi:10.1136/thoraxjnl-2017-210070
33. Domscheit H, Hegeman MA, Carvalho N, Spieth PM. Molecular dynamics of lipopolysaccharide-induced lung injury in rodents. *Front Physiol*. 2020;11:36. doi:10.3389/fphys.2020.00036
34. Patel BV, Wilson MR, Takata M. Resolution of acute lung injury and inflammation: a translational mouse model. *Eur Respir J*. 2012;39(5):1162-1170. doi:10.1183/09031936.00093911
35. Gefter WB, Lee KS, Schiebler ML, et al. Pulmonary functional imaging: part 2—state-of-the-art clinical applications and opportunities for improved patient care. *Radiology*. 2021;299(3):524-538. doi:10.1148/radiol.2021204033
36. Rankine LJ, Wang Z, Wang JM, et al. ^{129}Xenon gas exchange magnetic resonance imaging as a potential prognostic marker for progression of idiopathic pulmonary fibrosis. *Ann Am Thorac Soc*. 2020;17(1):121-125. doi:10.1513/AnnalsATS.201905-413RL
37. Myc L, Qing K, He M, et al. Characterisation of gas exchange in COPD with dissolved-phase hyperpolarised xenon-129 MRI. *Thorax*. 2021;76(2):178-181. doi:10.1136/thoraxjnl-2020-214924
38. Zhang H, Xie J, Xiao S, et al. Lung morphometry using hyperpolarized ^{129}Xe multi-b diffusion MRI with compressed sensing in healthy subjects and patients with COPD. *Med Phys*. 2018;45(7):3097-3108. doi:10.1002/mp.12944
39. Ouriadov A, Fox M, Hegarty E, Parraga G, Wong E, Santyr GE. Early stage radiation-induced lung injury detected using hyperpolarized (129) Xe morphometry: proof-of-concept demonstration in a rat model. *Magn Reson Med*. 2016;75(6):2421-2431. doi:10.1002/mrm.25825
40. Zhang H, Li X, Liao S, et al. SPLUNC1 knockout enhances LPS-induced lung injury by increasing recruitment of CD11b+ Gr-1+ cells to the spleen of mice. *Oncol Rep*. 2018;39(1):358-366. doi:10.3892/or.2017.6063

41. de Souza Xavier Costa N, Ribeiro Júnior G, dos Santos Alemany AA, et al. Early and late pulmonary effects of nebulized LPS in mice: an acute lung injury model. *PLoS ONE*. 2017;12(9):e0185474. doi:10.1371/journal.pone.0185474
42. Izbicki G, Segel M, Christensen T, Conner M, Breuer R. Time course of bleomycin-induced lung fibrosis. *Int J Exp Pathol*. 2002;83(3):111-119. doi:10.1046/j.1365-2613.2002.00220.x

How to cite this article: Zhang M, Li H, Li H, et al. Dynamic evaluation of acute lung injury using hyperpolarized ^{129}Xe magnetic resonance. *NMR in Biomedicine*. 2024;37(4):e5078. doi:10.1002/nbm.5078